Journal of Cleaner Production 170 (2018) 242–250

Contents lists available at ScienceDirect

Journal of Cleaner Production

journal homepage: www.elsevier.com/locate/jclepro

Photocatalytic carbon dioxide reduction to fuels in continuous flow monolith photoreactor using montmorillonite dispersed Fe/TiO_2 nanocatalyst

Muhammad Tahir [a, b, *]

[a] Chemical Reaction Engineering Group (CREG), Department of Chemical Engineering, Faculty of Chemical and Energy Engineering, Universiti Teknologi Malaysia (UTM), 81310, UTM Johor Bahru, Johor, Malaysia
[b] Department of Chemical Engineering, COMSATS Institute of Information Technology, Lahore, Pakistan

ARTICLE INFO

Article history:
Received 28 February 2017
Received in revised form
12 September 2017
Accepted 12 September 2017
Available online 17 September 2017

Keywords:
Photo-catalysis
Cleaner CO_2 reduction
Montmorillonite
Monolith photo-reactor

ABSTRACT

Photocatalytic conversion of CO_2 to fuels has attracted immense attention because it offers a cleaner energy technology and safer environment. In this study, performance of structured montmorillonite (MMT) dispersed Fe-doped titanium dioxide (Fe/TiO_2) nanocomposite was tested for dynamic photo-induced CO_2 reduction by H_2 to fuels. Cordierite monolithic support was employed in order to improve the photo-activity and reusability of Fe-MMT/TiO_2 nanocomposite in a CO_2 utilization process. MMT-clay supported Fe/TiO_2 samples were prepared by a controlled and direct sol-gel method and were dip-coated over the monolith micro-channels. The efficiency of Fe-loaded MMT/TiO_2 for CO_2 reduction by H_2 toward CO was investigated using a cell type and a monolith photo-reactor under UV-light. The maximum CO yield over 3 wt % Fe-10 wt % MMT-loaded TiO_2 catalyst reached 166 μmole g-catal.$^{-1}$ h^{-1} at selectivity 99.70%, considerably higher than the amount of CO produced over the MMT/TiO_2 (16 μmole g-catal.$^{-1}$ h^{-1}) and the pure TiO_2 (5 μmole g-catal.$^{-1}$ h^{-1}) catalysts. The other products observed with adequate amounts were CH_4 and C_2H_6. More importantly, photo-activity and stability of Fe-MMT/TiO_2 catalyst for CO evolution was significantly improved using monolith photo-reactor compared to the cell type reactor under the same operating conditions. This enactment was evidently due to higher quantum efficiency of monolith photoreactor, improved adsorption-desorption process in a catalyst coated monolith channels and hindered charges recombination by Fe. The reusability of catalyst loaded over the monolithic support showed greater recycling capability than the catalyst dispersed in a cell reactor. This development confirmed higher photo-activity of Fe-MMT/TiO_2 photo-catalyst loaded over monolithic support for CO_2 photo-reduction to cleaner fuels.

1. Introduction

Global warming caused by the drastic release of CO_2 concentration in the atmosphere induced by burning of fossil fuels has drawn considerable attention to the need to address environmental challenges related to climate change (Alaba et al., 2017). Solving CO_2 problems requires cleaner technologies that could be used for the permanent production of hydrocarbon resources with reduced emissions, less waste and greater cost effectiveness (Yong et al., 2016). The conversion of CO_2 to fuels using environment friendly technology, which could not only replace conventional energy resources but can provide opportunity for green and sustainable development, is gaining increasing attention (Kiatphuengporn et al., 2017). Since CO_2 is a rather inert and stable molecule, its reduction is a challenging task because of involving higher input energy (Yang and Xu, 2016). Therefore, the use of cleaner photo-technology for the conversion of CO_2 to fuels such as CH_3OH (Yu et al., 2015), CH_4 (He et al., 2016) and CO (Tahir and Amin, 2016) by the use of light irradiation is considered an attractive pathway toward economical and sustainable process. However, lower yield rates and selectivity has been reported as H_2O is difficult to reduce. Thermodynamically, photocatalytic CO_2 reduction with H_2O is not a favorable process, because reduction of H^+ released from H_2O,

* Corresponding author. Chemical Reaction Engineering Group (CREG), Department of Chemical Engineering, Faculty of Chemical and Energy Engineering, Universiti Teknologi Malaysia (UTM), 81310, UTM Johor Bahru, Johor, Malaysia.
E-mail addresses: mtahir@cheme.utm.my, bttahir@yahoo.com.

https://doi.org/10.1016/j.jclepro.2017.09.118
0959-6526/

usually competes with CO_2 reduction. Recently, H_2 as a potentially viable reductant for CO_2 reduction to fuels over different type of photocatalysts has been reported (Tahir et al., 2016). Therefore, it is appropriate to investigate H_2 as a reductant for photocatalytic reduction of CO_2 to cleaner fuels.

Among the various semiconductor materials, titanium dioxide (TiO_2) has attracted many researchers in recent years due to its rewards such as abundant availability at low cost, chemical/thermal stability, resistance to chemicals and high oxidative potential (Paulino et al., 2016). However, its poor photocatalytic activity due to fast charge carrier recombination rate is a great challenge. In recent years, various attempts have been made to improve TiO_2 photoactivity by modifying its structure with metals, non-metals, coupling with other semiconductors and co-catalyst modifications. However, all these approaches have economic limitations and cleaner environment aspects.

One prospective path to enhance TiO_2 activity is by its dispersion into clay micro-sheets. Recently, natural clay minerals are considered low-cost and environmentally friendly materials and can be employed to develop clean technology for various applications. Among the naturally available clays, montmorillonite (MMT) is most widely used to develop clay-semiconductor nanocomposite in photo-catalysis applications. MMT is a pillared clay which has tremendous potential for adsorption and as a support for semiconductor materials due to favorable microporous structure with high metal dispersion, high cations exchange capacity, superior charge trapping ability and provides prolonged stability (Mulewa et al., 2017). Previously, enhanced photocatalytic CO_2 reduction over MMT/TiO_2 nanocomposite for the production of CO with improve photo-activity and selectivity has been described (Tahir et al., 2015b). Similarly, ZnS/MMT nanocomposites with enhanced photocatalytic performance in CO_2 reduction was reported (Kočí et al., 2014). The activity of MMT/TiO_2 nanocomposite can be further improved by loading suitable metal ions (Tahir, 2017). In this viewpoint, various transition metal ions (e.g., Fe) incorporating in TiO_2 were investigated with improved charges separation rate (Kong et al., 2017). The ferric species, the imperative component of Fenton reagent, have been tested to be suitable to improve photo-activity of semiconductors (Chen et al., 2017b). Fe-ions incorporated TiO_2 catalyst have been tested for degradation of pollutants with enhanced photoactivity by Fe while using UV/visible light. The enhanced photo-activity was evidently due to promoting Fe/TiO_2 interfacial charge transfer process (Harifi and Montazer, 2014). Due to superior charge transfer separation in semiconductors by Fe, it is appropriate to explore further for photocatalytic CO_2 reduction to cleaner fuels.

On the other hand, photo-catalysis process is considered efficient only if there is effective interaction between the light irradiations, catalyst and reactants (Tahir et al., 2015a). To date, slurry type reactors have limitations such as poor light utilization efficiency, the loss of catalyst during recycling, high cost of catalyst separation and lower intensity to stimulate complex nature of reaction (Ola et al., 2012). Currently, immobilized photocatalytic systems, in particular, monolithic supports, have been found very efficient for CO_2 reduction to CO with enhanced yield and selectivity (Tahir and Amin, 2016). This is because of their unique structure and enhanced photonic efficiency (Yuan et al., 2014). In the recent literature, application of Fe-promoted TiO_2/MMT nanocomposites for the conversion of CO_2 to CO with H_2 as a reducing agent in a monolith photo-reactor has not been reported.

In this context, further research involving MMT supported Fe/TiO_2 photo-catalyst for gas phase CO_2 conversion in a continuous monolith photo-reactor to produce renewable and cleaner fuels is warranted. In this study an attempt has been made to use low-cost and green catalyst to improve economic and environmental aspects towards cleaner fuels production. Herein, structured MMT-clay modify TiO_2 promoted by Fe has been synthesized by sol-gel method and was immobilized onto monolith micro-channels. The photo-activity test of the nanocomposites was investigated for selective and enhanced photocatalytic CO_2 reduction in a continuous flow photo-reactor. Performance analysis of a cell type and a monolith photo-reactor to apprehend the role of support and catalyst on the activity and selectivity of catalyst toward cleaner fuels has been critically investigated. Stability analysis of nanocomposite catalysts was conducted in a cell type and monolith photo-reactor to evaluate the life of catalyst. The reaction mechanism for photo-induced CO_2 reduction to CO over Fe-MMT/TiO_2 catalyst is proposed based on the experimental data.

2. Experimental

2.1. Catalyst preparation

Commercially available tetra-isopropyl orthotitanate (98%, Merck), montmorillonite (1.4 P, Sigma-Aldrich) and $FeCl_3$ (Sigma-Aldrich) were used without further purification. Structured MMT dispersed Fe-loaded TiO_2 nanocomposites were synthesized through a facile single step sol-gel method. Typically, 20 mL titanium solution dispersed in 45 mL isopropanol was taken into flask for the hydrolysis process. The solution was hydrolysed by adding 15 mL acetic acid (1 M) under stirring. After 12 h stirring, the appropriate quantity of $FeCl_3$ was added to above solution under stirring. Next, fixed quantity of MMT-clay was dispersed in isopropanol by stirring 1 h, then added into Fe/titanium solution and the mixture stirred for another 6 h to complete the intercalation process. Finally, clear thick titanium sol was transferred into glass container for coating monolith substrate.

The monolith used were cordierite in structure with 200 channels per square inch (CPSI), 6 cm diameter and 2 cm length. After washing with water and acetone to remove impurities, all the monoliths were dried at 110 °C overnight before initial weight was calculated. To ensure the accuracy of the results, three readings were recorded for the bare and coated monoliths, the resultant was catalyst weight loaded over the channels. For catalyst coating, weighed monoliths were dipped for 10 s, removed, and then blown off with hot compressed air to get fine catalyst coating layer over the channels surface. The amount of catalyst loading can be increased by repeating the same procedure. Finally, catalyst coated monoliths were put in the oven and dried at 80 °C for 12 h before calcining at a temperature of 500 °C for duration of 5 h. The schematic presentation of catalyst coating over the monolith channels is depicted in Fig. 1.

2.2. Catalyst characterization

X-ray Diffraction (XRD) analysis of the samples was conducted using a Bruker D8 advance diffractometer equipped with Cu− Kα radiation ($\lambda = 0.154$ nm). The data was obtained at 40 kV and 40 mA in the scan range of $10^\circ \leq 2\theta \leq 80^\circ$, 1.2° per min scan speed, and 0.02° step size. The samples morphology was inspected using Field Emission Scanning Electron Microscopy (FE-SEM) employing a JEOL JSM6390 LV SEM. High Resolution Transmission Electron Microscope (HRTEM) (FEI-Tecni G2) was used to obtain mesoporous and lattice structure of the samples. N_2 adsorption-desorption isotherms were obtained at −196 °C using Micrometric ASAP 2020 analyser before samples were degasified at 250 °C for 4 h under vacuum. Fourier Transformed Infrared (FT-IR) Spectrometer peaks were obtained in the range of 400–4000 cm^{-1} employing Spectrum 2000 Explorer Spectrometer. Diffuse reflectance spectra (DRS) of the powder samples were collected by employing Agilent, Cary

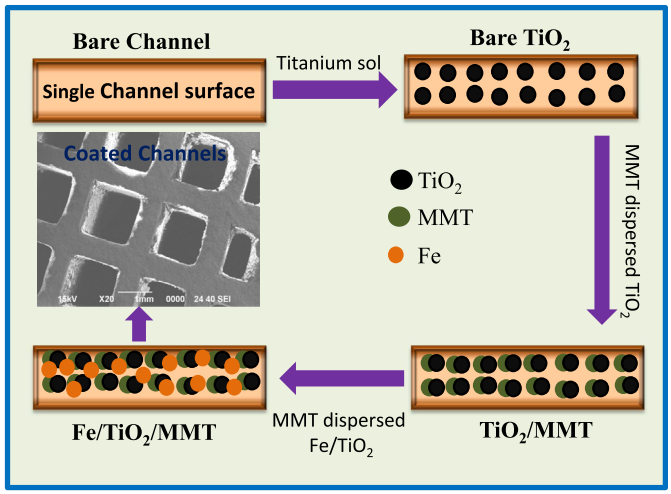

Fig. 1. Scheme for the preparation of MMT-dispersed Fe/TiO_2 nano-catalyst coated over monolithic support.

100 UV–Vis spectrophotometer. The instrument was equipped with integrated sphere assembly to analyse powder samples and absorbance spectra were measured in the 200–800 nm wavelength range.

2.3. Photocatalytic activity test

The activity of photo-induced CO_2-hydrogen reaction system was tested in a gas phase continuous flow photo-reactor as depicted in Fig. 2. The reactor consists of cylindrical vessel having 150 cm^3 total volume and quartz glass window of thickness 8 mm was used for passing light irradiation. Located at the top of the reactor, a 200 W Hg reflector lamp was used as a source, having a maximum light intensity 150 mW cm^{-2} at wavelength 252 nm, measured at the top of glass window. The cooling fans were used to remove lamp heat and aluminium foil was used to cover the reactor. The gas feed rates were controlled using online mass flow controllers (MFC) with gas flow measurements. A gas mixture was used to ensure all the gases were uniformly mixed before entering into the reactor. The temperature of the reactor was controlled using temperature controller while pressure was measured using pressure gauge.

In case of CO_2 reduction in a cell type photo-reactor, 25 mg powder catalyst suspended uniformly inside the reactor to confirm effective light distribution over the catalyst surface as illustrated in Fig. 2 (a). The schematics of monolith photo-reactor for CO_2-hydrogen reaction system is portrayed in Fig. 2 (b). Before starting the experiment, the reactor was purged with feed gas mixture (CO_2 and H_2, purity = 99.99%) flowing continuously at total flow rate 20 mL/min. The feed mixture (CO_2/H_2) molar feed ratio of 1.0 was fixed while flow rate of 20 mL/min was adjusted for each gas. Continuous flow mode was used in all the experiments at atmosphere pressure. Gas chromatograph (GC-Agilent Technologies 6890 N, USA) equipped with thermal conductivity detector (TCD) and a flame ionized detector (FID) was used for the products analysis. In addition, HP-PLOT Q capillary column (Agilent, length 30 m, ID 0.53 mm, film 40 μm) was connected with FID detector, while Porapak Q and Mol Sieve 5A columns were connected to TCD detector.

3. Results and discussion

3.1. Catalyst characterization

XRD plots of TiO_2, MMT and Fe-loaded TiO_2 nano-composites are shown in Fig. 3. The peaks of TiO_2 calcined at 500 °C revealed a pure anatase and crystalline phase. The XRD analysis of MMT presents a broad basal reflection of (0 0 1) at $2\theta = 3.70°$, originated due to stacking disorder of MMT layers. In the case of MMT and Fe-loaded TiO_2 samples, TiO_2 persisted its original reflection with no additional peak appeared, however, all TiO_2 peaks become broader and weaker. This was probably because MMT hindered TiO_2 crystal growth, resulting in reduced crystallite size (Tahir et al., 2015b). The prominent MMT peak (0 0 1) due to the layered clay has

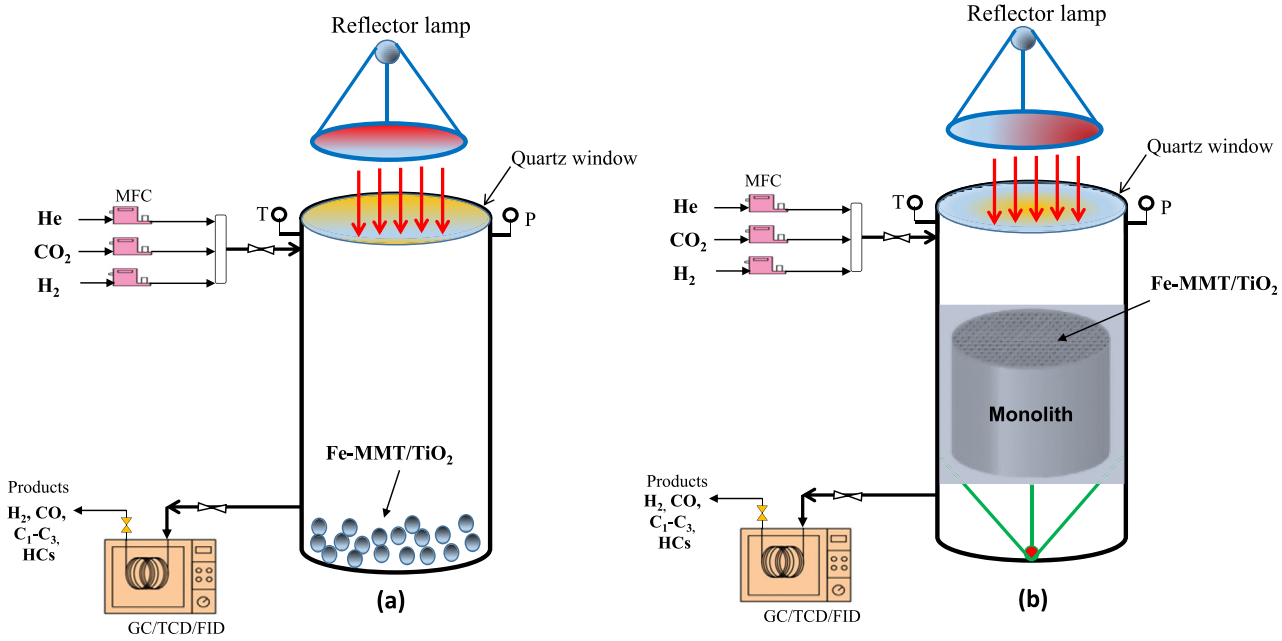

Fig. 2. Experimental set-up of cell and monolith photo-reactors for photocatalytic CO_2 reduction to fuels under light irradiation : (a) Cell photo-reactor, (b) Monolith photo-reactor.

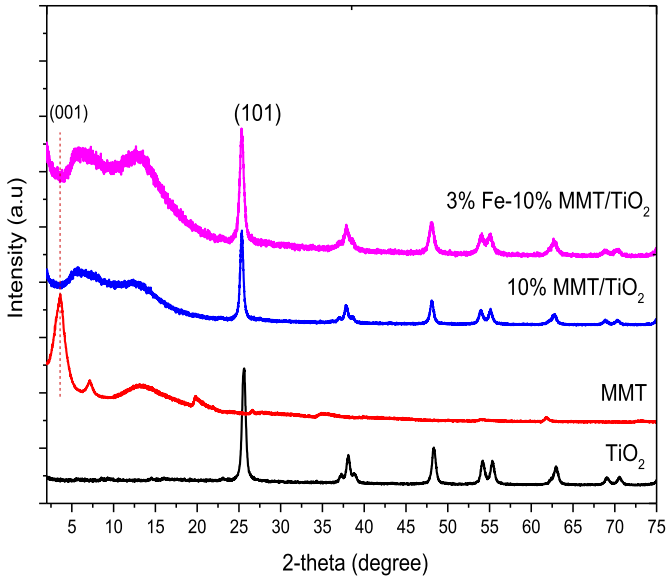

Fig. 3. X-ray diffraction patterns of TiO_2, MMT and Fe/MMT-modified TiO_2 catalysts.

disappeared in all MMT based samples. This revealed that the layered structure of the MMT has become disordered with uniform dispersion of TiO_2 NPs and similar observations were reported previously (Tahir et al., 2015b).

The morphology of cordierite support was investigated by SEM as demonstrated in Fig. S1. The bare monolith channels of cordierite structure with channel diameter 1.52 mm are obvious in Fig. S1 (a). Fig. S1 (b) reveals uniformly coated catalysts over the channels surface with no broken layers. This indicates a good dispersion of catalysts over the monolith surface with sol-gel dip-coating method.

The morphology of TiO_2 and Fe/MMT modified TiO_2 samples is presented in Fig. S2. Fig. S2 (a) reveals spherical shape and uniform size of TiO_2 nanoparticles. The MMT image in Fig. S2 (b) shows stacked MMT layers with disorder structure. Fig. S2 (c) illustrates images of TiO_2 dispersion over the MMT layers and Fe-loaded MMT/TiO_2 samples. Evidently, MMT layers were completely destroyed and TiO_2 NPs are well distributed over the MMT surface, producing MMT/TiO_2 nanocomposite. The morphology of Fe-loaded MMT/TiO_2 sample is very similar to MMT/TiO_2 composite, where MMT layers are destroyed as presented in Fig. S2 (d). These observations have confirmed well-developed MMT-dispersed Fe/TiO_2 nanocomposite.

The transmission electron microscopy (TEM) images of MMT-dispersed TiO_2 sample are shown in Fig. 4. Fig. 4 (a) displayed uniform dispersion of TiO_2 nanoparticles inside MMT structure. The existence of TiO_2 inside MMT galleries and over the structure is obvious. The lattice fringe spacing of 0.35 nm was observed, corresponding to plan (1 0 1) of anatase TiO_2, as depicted in Fig. 4 (b). However, lattice planes of MMT was not detected, confirming its specific structure and uniform dispersion in TiO_2 structure (Li et al., 2015).

Fig. S3 presents FTIR peaks of TiO_2, MMT and Fe-loaded MMT/TiO_2 samples. The spectra of TiO_2 with bands appeared at 1616 cm^{-1} and 3408 cm^{-1}, indicating chemisorbed H_2O in TiO_2 and −OH stretching vibration. The MMT spectra showed various peaks at different locations. The stretching band at 3633 cm^{-1} was attributed to Al_2OH group of octahedral layer in MMT, while peaks at 3428 cm^{-1} and 1625 cm^{-1} pertain to stretching and bending vibration of hydroxyl group of water molecules on the external layer of MMT. Furthermore, C−H stretching vibration of the organic modifiers in MMT structure appeared at 2926 cm^{-1} and 2829 cm^{-1}. Asymmetric vibration of SiO_2 tetrahedral layer in MMT can be identified at 1049 cm^{-1}, with several peaks at 1000 and 500 cm^{-1} attributed to Al-IV tetrahedra. The stretching vibration bands of MMT/TiO_2 and Fe-MMT/TiO_2 have similar reflections to the pure TiO_2 with stretching band at 1049 cm^{-1} due to asymmetric stretching vibration of SiO_2 tetrahedra (Li et al., 2015).

Fig. S4 depicts N_2 adsorption-desorption analysis of MMT, TiO_2 and Fe-loaded MMT/TiO_2 samples. All the isotherms show a type IV with high volume of N_2 adsorption in a high relative pressure (P/Po) region. Monolayer/multilayer adsorption on the internal surface of pores is obvious at initial part of the isotherms, where pressure is relatively low (low P/Po). On the other hand, capillary condensation is obvious on the upper part of isotherms at relatively high pressure (high P/Po).

Table 1 presents summary of surface areas, pore volumes and pore sizes of TiO_2 and Fe-loaded MMT/TiO_2 samples. The specific surface area (S_{BET}) of 43 $m^2\ g^{-1}$ was obtained in the case of pure TiO_2, increasing to 52 $m^2\ g^{-1}$ for 10 wt % MMT/TiO_2 sample. On the other hand, BET surface area gradually decreased to 45 $m^2\ g^{-1}$ when 3 wt % Fe-loaded to 10% MMT/TiO_2 nanocomposites, respectively. However, BJH surface area significantly increased in Fe-loaded MMT/TiO_2 samples, confirming mesoporous structure of these materials. Similar observations could be seen in BJH adsorption pore volumes. In addition, pore diameter of pure TiO_2 was 11 nm, decreased to 9 nm in MMT and Fe-loaded MMT/TiO_2 samples. This revealed MMT has an impact on the crystal growth of

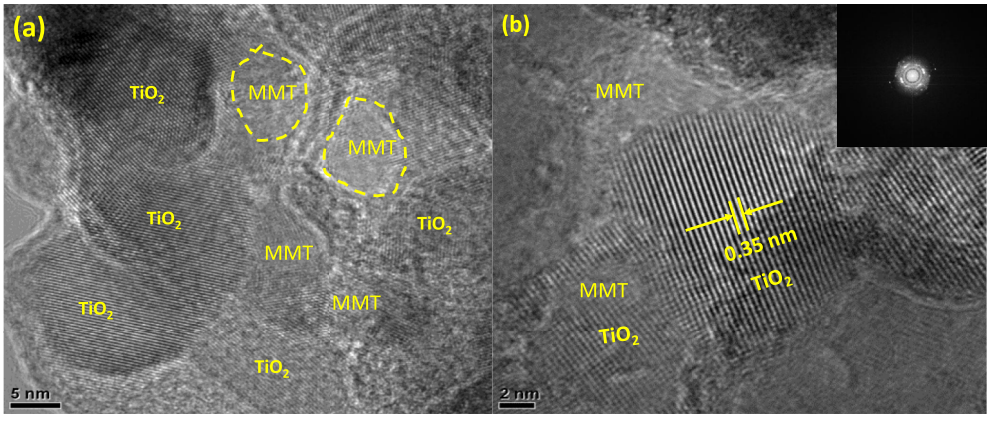

Fig. 4. TEM images of MMT-dispersed TiO_2 nanoparticles: (a) TEM image with TiO_2 dispersed over MMT, (b) d-spacing of TiO_2 with electron dispersion (insert inage).

Table 1
Summary of physiochemical analysis of TiO_2 and Fe/MMT supported TiO_2 samples.

Sample	BET surface area (m^2/g)	BJH pore area (m^2/g)	BJH pore volume (cm^3/g)	Pore width (nm)	Band gap energy eV
TiO_2	43	52	0.135	11	3.11
10% MMT/TiO_2	52	48	0.103	9	3.10
3% Fe-10% MMT/TiO_2	45	60	0.113	9	3.07

TiO_2, resulting in improved morphology.

UV–Vis diffuse reflectance spectra (DRS) of TiO_2, MMT/TiO_2 and Fe-modified MMT/TiO_2 samples are shown in Fig. S5. The absorbance spectra for both TiO_2 and MMT/TiO_2 indicates light absorption under UV-light irradiation. However, in Fe-loaded MMT/TiO_2 samples, it is shifted toward visible region. The direct band gap energy, according to plot of $(\alpha h\nu)^2$ vs. photon energy (eV), is summarized in Table 1. TiO_2 and MMT/TiO_2 have a direct band gap of 3.11 and 3.10 eV, respectively. The TiO_2 band gap energy has decreased to 3.07 eV in Fe-loaded MMT/TiO_2 samples, possibly due to the reduced crystallite size of TiO_2 nanoparticles.

3.2. Photocatalytic CO_2 reduction with H_2 in monolith photo-reactor

Before photocatalytic CO_2 reduction experiments, quality control analysis were conducted to confirm products were originated during photo-reduction of CO_2 only. All the catalysts were tested in gas phase system using high purity helium. Using only helium gas (in the absence of CO_2 and H_2), carbon containing compounds were not detected by the catalyst samples under light energy. Therefore, all the products in the experiments must be produced from CO_2 reductants through photocatalytic reaction. In addition, all the experiments were performed in triplicate and average values have been reported.

The effects of MMT onto TiO_2 performance for CO_2 photo-reduction with H_2 to CO and CH_4 is presented in Fig. 5 (a). Evidently, CO was detected as the main product over all types of photo-catalysts, which has confirmed favorable reaction over the pure TiO_2 and MMT modified TiO_2 samples while using monolith as the photo-reactor and hydrogen as a reducing agent. Pure TiO_2 has low photo-activity for CO production, which gradually increased in MMT supported TiO_2 samples. This was evidently due to high illuminated active surface area with hindered charges recombination rate and efficient CO_2 adsorption in MMT/TiO_2 samples loaded over monolith microchannel. Adding MMT into TiO_2 resulted in significantly improved CO_2 photo-reduction efficiency with optimum MMT-loading of 10 wt %. Therefore, 10 wt % MMT-loaded TiO_2 sample was the most active for dynamic CO evolution. However, with more MMT loading (e.g., 15 wt %) into TiO_2, photo-activity was gradually reduced. This was certainly due to reduce in photo-catalyst (TiO_2) active sites and possibly due to shading effect inside the monolith micro-channels by excessive MMT-loading.

The effect of Fe-loading on the photo-activity of MMT/TiO_2 for selective photocatalytic CO evolution at different irradiation time is presented in Fig. 5 (b). Noticeably, much higher CO production was detected over Fe-loaded MMT/TiO_2 compared to MMT/TiO_2 and pure TiO_2 samples. This considerably improved photo-activity of Fe-loaded TiO_2 samples was evidently due to efficient charges separation with hindered recombination rate by Fe. Since CO_2 was reduced in a continuous flow monolith photo-reactor, the production of CO did not persist over the irradiation time and gradually reduced to steady state.

The performance of Fe on the photo-activity of MMT/TiO_2 for photocatalytic CO_2 conversion with H_2 to CH_4 and C_2H_6 is presented in Fig. 6. Using pure TiO_2, only small amount of CH_4 was produced, which was gradually increased in Fe-loaded MMT/TiO_2 samples as depicted in Fig. 6 (a). On the other hand, C_2H_6 production was not detected in the pure TiO_2 but its production was evidenced in MMT/TiO_2 and Fe-MMT/TiO_2 samples as presented in Fig. 6 (b). The prominent C_2H_6 production in the presence of Fe was possibly due to instant charge separation resulting in prolonged recombination time of the photo-generated charges (Harifi and Montazer, 2014).

The yield rate and selectivity of different products are presented in Table 2. The yield of CO over 3% Fe-10 wt % MMT/TiO_2 was 166 μmole g-catal.$^{-1}$ h^{-1}, 10 times more than the 10 wt % MMT/TiO_2 and 33 fold more than the amount produced over the pure TiO_2. The enhanced photo-activity was noticeably due to fast charges transfer rate by Fe with larger active surface sites over monolith channels

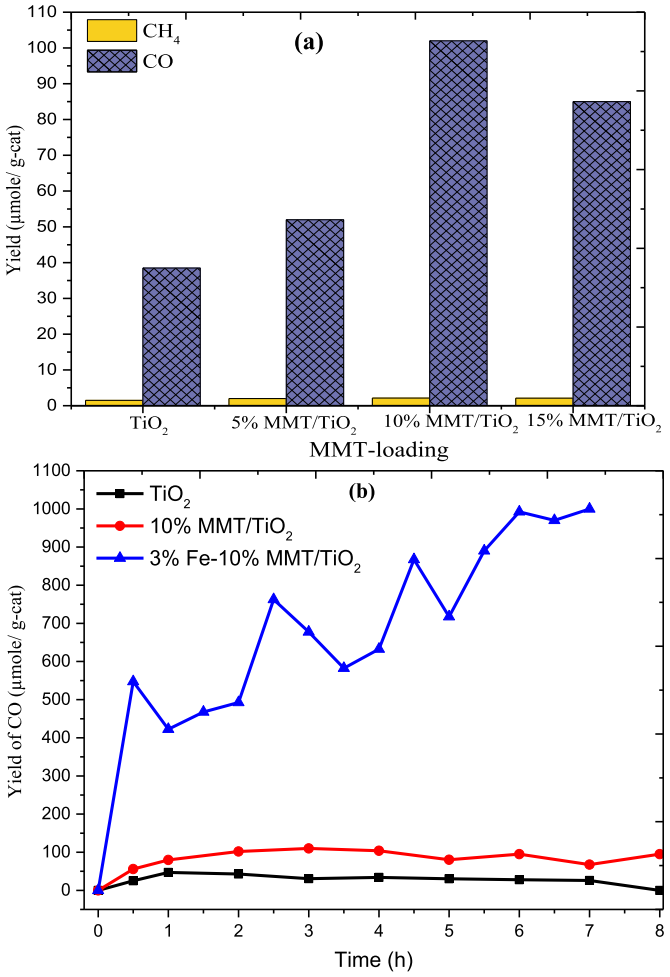

Fig. 5. (a) Effect of MMT loading onto TiO_2 activity for CO_2 reduction with H_2 in a monolith photo-reactor; (b) Dynamic CO evolution over Fe-TiO_2/MMT samples during CO_2 reduction with H_2 at 100 °C and CO_2/H_2 feed ratio 1.0 and feed flow rate 20 mL/min.

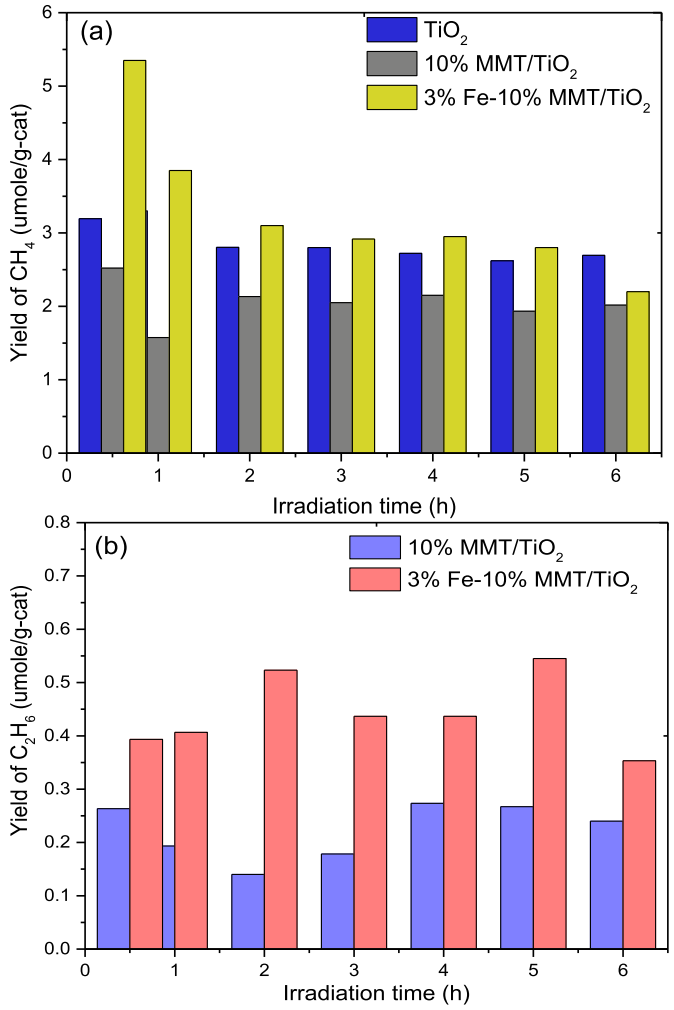

Fig. 6. Effect of Fe-loading onto MMT/TiO_2 activity for CO_2 reduction with H_2 to hydrocarbons; (a) CH_4 evolution, (b) C_2H_6 evolution at 100 °C, CO_2/H_2 ratio 1.0 and feed flow 20 mL/min.

(Tahir and Tahir, 2016). The selectivity for CO production over the TiO_2 increased from ~91.74 to 99.70% in Fe-loaded MMT/TiO_2 sample. These results show that CO_2 can efficiently be converted to cleaner fuels using Fe-loaded MMT/TiO_2 catalyst and monolith photo-reactor.

3.3. Performance analysis of cell type and monolith photo-reactor

The performance of TiO_2 catalyst loaded with Fe and MMT was further investigated using a cell type and monolith photo-reactors operating in a continuous operation at CO_2/H_2 feed ratio 1.0. The yield of CO production in a cell type and monolith photo-reactor over the irradiation time is presented in Fig. 7 (a). Using cell type reactor, yield of CO produced over Fe-loaded MMT/TiO_2 composite was significantly higher than using only Fe/TiO_2 catalyst over the entire irradiation. This revealed that MMT-dispersed Fe/TiO_2 is more efficient for reduction of CO_2-to-CO than using only Fe/TiO_2 catalyst. This significant enhancement in photo-activity by MMT could be explained based on their CO_2 adsorption capacity with more mobility of photo-generated charges. In the presence of Fe and MMT, there was more transport of charges toward CO_2, resulting in enhanced yield and product selectivity. Similarly, there was a significant effect of monolithic support on the activity of photo-catalyst. The amount of CO produced using Fe-promoted MMT/TiO_2 nanocomposite loaded on the monolithic support was much higher than the CO produced in a cell type photo-reactor in which catalyst was dispersed over the reactor surface. This significantly enhanced photo-activity in a monolith photo-reactor was evidently due to improved illuminated active surface area with efficient utilization of light irradiations and more dynamic adsorption-desorption of species over the catalyst coated monoliths.

The production of CH_4 in a cell type and monolith photo-reactor over Fe and MMT modified catalyst at different irradiation time is depicted in Fig. 7 (b). Initially, increased yield rate of CH_4 production detected with Fe-MMT/TiO_2 catalyst in a cell type photo-reactor but yield gradually declined over the irradiation time. The photo-activity of Fe/TiO_2 catalyst for CH_4 production revealed its suitability for CH_4 production over the entire irradiation time. On the other hand, there was continuous production of CH_4 in a monolith photo-reactor. This revealed cell type reactor promoted CH_4 production while monolith reactor is favorable for CO production. These observations could be explained based on the efficient adsorption-desorption process in the catalyst coated over monolithic support. In general, using cell type photo-reactor, desorption of reactants was not very fast, CO adsorbed over the catalyst was finally converted to CH_4. However, in a monolith photo-reactor, these processes were very fast, thus only small amount of CH_4 was detected and similar observations eminent with the irradiation time as already reported previously (Tahir and Amin, 2016). However, experimental limitations should be considered to get consistent results which include: (a) catalyst loaded inside monolith channels should be uniform to get higher efficiency and selectivity of the products; and (b) lamp used as a source of light irradiations should be a reflector type to get enough intensity for passing light irradiations through monolith microchannel.

The stability of MMT-dispersed Fe/TiO_2 catalyst was further investigated to evaluate life of catalyst in a cell type and monolith photo-reactors operating in continuous mode. For stability analysis of catalysts, experiments were conducted in cyclic runs under identical conditions. Before starting the next cyclic run of the used catalyst, the reactor was flushed with pure helium gas. Fig. 8 (a) presents stability analysis for photocatalytic CO_2 reduction with H_2 to CO over 3 wt % Fe-loaded MMT/TiO_2 catalyst. In the first run, CO production was higher using cell type reactor, but in second and third runs, it was gradually decreased over all irradiation times. However, a stable and continuous production of CO could be observed with the catalyst loaded in a monolith photo-reactor. Therefore, the photo-catalyst immobilized onto monolithic support provides prolonged stability in cyclic runs compared to distribute over the surface of cell type reactor. The decrease in activity of photo-catalyst in a cell type photo-reactor might be due to less efficient adsorption-desorption process and catalyst losing its activity due to reaction only over the surface compared to catalyst loaded over the monolithic support as depicted in Fig. 8 (b). These

Table 2
Summary of yield rates and selectivity of products over TiO_2 and Fe/MMT modified TiO_2 samples.

Samples	Yield rate[a] μmole g-catal.$^{-1}$h^{-1}			Selectivity (%)	
	CO	CH_4	C_2H_6	CO	CH_4
TiO_2	5	0.45	–	91.74	8.26
10% MMT/TiO_2	16	0.33	0.04	97.94	2.02
3% Fe-10% MMT/TiO_2	166	0.40	0.10	99.70	0.24

[a] Yield rate calculated based on 6 h irradiation time.

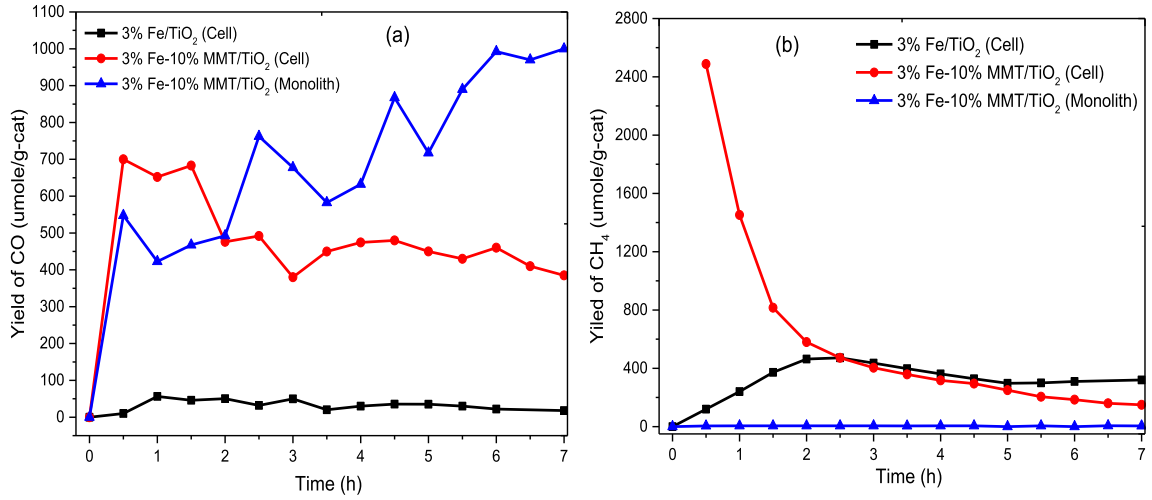

Fig. 7. Performance analysis of cell type and monolith photo-reactor; (a) Yield of CO, (b) Yield of CH_4.

results confirmed higher photoactivity and stability of Fe-loaded MMT/TiO_2 catalyst loaded in a monolith photoreactor.

3.4. Transition of CO_2 photo-conversion to cleaner fuels

At present, photocatalytic conversion of CO_2 into value added chemicals including CO, CH_4 and CH_3OH has been considered as one of the top research areas in the world. This process can deal with the mitigation of CO_2 associated global warming problem, the creation of highly sustainable and cleaner energy resources, and development of one of the best clean processes to store energy with sufficiently high energy density in comparison to all the existing methods of energy storage. The process for converting CO_2 into cleaner fuels can be developed by careful analysis and understanding of the information available on this process reported so far in the literature for future applications. An approximate comparison of CO_2 photo-conversion for the transformation of photo-energy to chemical energy by various semiconductor catalyst is given in Table 3. Note that CO_2 can be converted to CO, CH_3OH and hydrocarbons over various TiO_2 based photo-catalysts under UV and visible light irradiations in different types of photo-reactors.

An ideal photo-catalyst possesses the following qualities: high activity, selectivity, and stability of catalyst under light irradiations with low cost and safer to the environment. In addition, photo-reactor design should provide larger illuminated active surface to absorb light irradiation, and enhanced interactions between reactants and photons of light energy. While photo-catalytic catalytic reduction of CO_2 has been relatively well-studied by different research groups, the effects of green clay materials in TiO_2 composite coupling with the monolith photoreactor in order to gain a better comprehension of the process chemistry and mechanisms involved has never been reported. However, present work reports significant amount of CO production from CO_2 by the use of Fe-loaded MMT/TiO_2 nanocomposite catalyst in a continuous flow monolith photoreactor. Thus, the use of cleaner photo-technology for CO_2 conversion to fuels can provide alternative pathways for the production of sustainable fuels with low cost and safer environment. Ideally, this technology provides an opportunity to reduce CO_2 under light irradiation. At the same time, it is green and clean. This process produces no waste material to pollute environment and produces high energy density clean fuels which may solve the problem of energy shortage in the future.

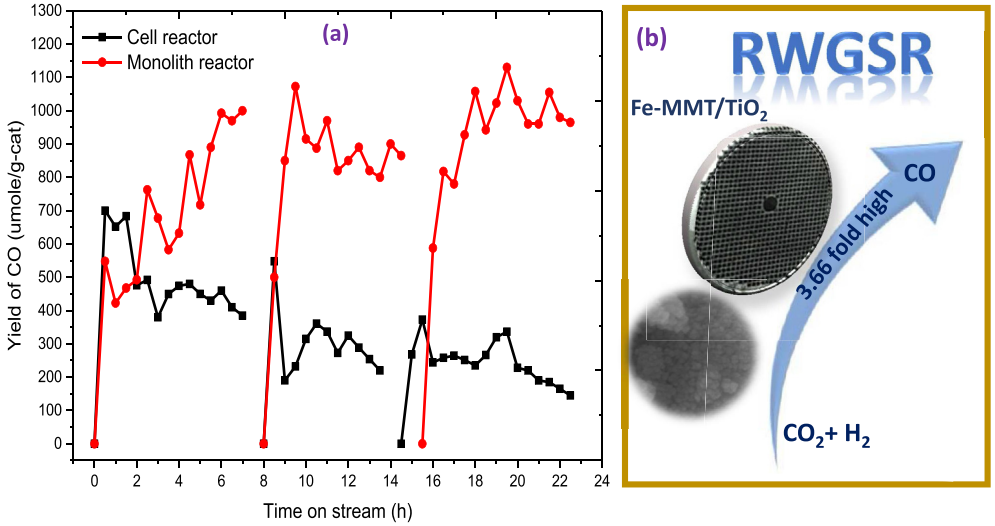

Fig. 8. (a) Stability studies of CO production during CO_2 reduction with H_2 over Fe-loaded MMT/TiO_2 composite in a cell type and monolith photo-reactor, (b) Schematic of enhanced CO_2 reduction via RWGS reaction in monolith photoreactor.

Table 3
Summary of literature for photocatalytic CO_2 conversion to fuels over different photo-catalysts.

Catalyst	Feed and light used	Reactor and parameters	Products	Remarks	Ref.
Fe-MMT/TiO_2	CO_2–H_2, Feed ratio = 1.0, 200 W Hg lamp, I = 150 mW/cm^2	Continuous flow monolith photoreactor, Volume = 150 cm^3, Fed flow rate = 20 mL/min, T = 100 °C	CO, CH_4, C_2H_6	CO was detected as main product with yield 166 μmole g-cat.$^{-1}$ h^{-1} at selectivity 99.70%.	Present study
Ce-La/TiO_2	CO_2–H_2O, 15 W fluorescent lamp, NaOH = 0.2 M,	Batch annular reactor, Volume = 500 mL, Catalyst loading = 1 g/L	CO, CH_4, CH_3OH	Maximum yield of 317.7 μmole g-cat.$^{-1}$ for CH_3OH in aqueous phase, while CH_4 and CO of 262.8 and 194.4 μmole g-cat.$^{-1}$ in gas phase were obtained over the period 6 h.	(Ali et al., 2017)
AuPd/3DOM-TiO_2	CO_2–H_2O, lamp = 300 W Xe lamp,	Gas-closed circulation system, I = 80 mW/cm^2,	CH_4, CO, H_2, O_2	CH_4 formation of 18.5 μmole g-cat.$^{-1}$ h^{-1} and selectivity 93.9%.	(Jiao et al., 2017)
V-W/TiO_2	CO_2–H_2O, 300 W Xenon lamp, I = 44.6 mW/cm^2,	Internally illuminated honeycomb monolith Pyrex glass reactor, Volume = 375 mL, T = 50 °C	H_2, CO, CH_4	Highest yields obtained were 1.91, 0.22 and 0.27 μmole g-cat.$^{-1}h^{-1}$ for	(Xiong et al., 2017a)
Ag/CdS	CO_2–H_2O, 300 W Xenon lamp,	Flask reactor, Volume = 80 mL,	CO, H_2	Production of CO of 1.29 μmole g-cat.$^{-1}$ and H_2 of 11 μmole g-cat.$^{-1}$ were obtained.	(Zhu et al., 2017)
TiO_2/HZSM-5/Fe	CO_2–H_2O, 300 W Xenon lamp,	Quartz reactor, Volume = 40 mL	CO, CH_4	Highest CO yield of μmole g-cat.$^{-1}h^{-1}$ was obtained.	(Tong et al., 2017)
ZnO/CeO	CO_2–H_2O, 300 W Xenon lamp, I = 63.7 mW/cm^2	Pyrex glass reactor, catalyst loading = 20 mg, T = 20 °C,	CO, CH_4	CO and CH_4 yields of 0.526 and 0.069 μmole g-cat.$^{-1}h^{-1}$ were obtained, respectively.	(Xiong et al., 2017b)
CdS/TiO_2/SBA-15@carbon paper	CO_2, NaOH aqueous solution, Xenon lamp, I = 20–140 mW/cm^2	Optofluidic membrane microreactor	CH_3OH,	NaOH and light intensity have positive effect on enhancing methanol production.	(Chen et al., 2017a)

3.5. Reaction mechanism for CO_2 reduction to fuels

During photocatalytic RWGS reaction, CO_2 is reacted with H_2 for the CO production with smaller amounts of CH_4 and C_2H_6 as the potential products using Fe-loaded MMT/TiO_2 composite catalyst. Therefore, possible reaction mechanism is depicted in Fig. 9 and illustrated in Eqs. (1)–(7) (Tahir and Amin, 2013).

$$TiO_2 \rightarrow e^- + h^+ \quad (1)$$

$$Fe^{3+} + 3e^- \rightarrow Fe \quad (2)$$

$$H_2 + 2h^+ \rightarrow 2H^+ \quad (3)$$

$$CO_2 + 2e^- \longrightarrow gCO_2^- \quad (4)$$

$$CO_2 + 2H^+ + 2e^- \rightarrow CO + H_2O \quad (RWGS) \quad (5)$$

$$CO_2 + 8H^+ + 8e^- \rightarrow CH_4 + 2H_2O \quad (6)$$

$$2CO_2 + 14H^+ + 14e^- \rightarrow C_2H_6 + 4H_2O \quad (7)$$

First, when the UV-light was irradiated to photo-catalyst, electron-hole pairs were produced (Eq. (1)). The photo-generated electrons were captured by Fe, resulting in their efficient separation (Eq. (2)). Next, electrons transferred toward CO_2 for its reduction while holes are consumed for H_2 oxidation as explained in Eqs. (3) and (4). Then, H^+ radicals and active electrons can reduce CO_2 to CO, CH_4 and C_2H_6 as explained in Eqs. (5)–(7). As discussed previously, CO was the main product with selectivity above 99%,

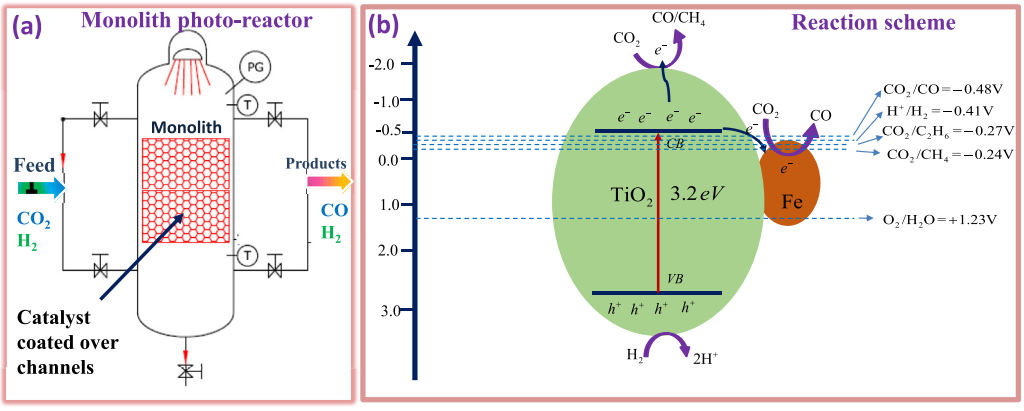

Fig. 9. Schematic of reaction mechanism for photocatalytic CO_2 reduction with H_2 to fuel in a monolith photoreactor: (a) Schematic of monolith reactor configuration, (b) Reaction scheme for CO_2 reduction.

confirming favorable CO_2 reduction process for CO production in a continuous flow monolith photo-reactor with Fe-loaded MMT/TiO_2 photo-catalysts. The significantly enhancement in CO yield rate over Fe/TiO_2 dispersed in MMT was clearly due to higher trapping of electrons by Fe, efficient CO_2 adsorption and enhanced light harvesting efficiency by monolith photoreactor.

This effective CO_2 utilization would lead to a promising solution not only for energy issues due to the use of light energy for high energy density cleaner fuels, but also produces less environmental pollution from CO_2 emission. Therefore, it can be concluded that the photo-technology integrated with monolith photoreactor has great potential application and it provides a green and sustainable innovation in chemical and petrochemical processes, and concurrently offers economic advantages in energy.

4. Conclusions

Montmorillonite clay dispersed Fe/TiO_2 nanocatalyst is a promising material for the reduction of CO_2 using a promising cleaner photo-technology. The photocatalytic CO_2 reduction was increased significantly by introducing Fe and MMT into TiO_2 loaded over monolithic support. The amount of CO as the key product produced over the Fe-MMT/TiO_2 nanocomposite was much higher when compared with pure MMT/TiO_2 and pure TiO_2 photo-catalyst. This enhancement in photocatalytic activity was perhaps due to delayed charges recombination rate by Fe and larger illuminated surface area in a monolith photo-reactor. The stability test revealed the prolonged activity of the photo-catalyst supported over the monolith micro-channels as compared to using cell photo-reactor. Therefore, cordierite monolithic support could improve photo-activity, selectivity and stability of Fe-MMT/TiO_2. Ideally, this technology provides a probability to reduce CO_2 to fuels by the use of light energy, a sustainable innovation in chemical and petrochemical processes. It has no waste material produced to pollute environment and produces the clean energy which may solve the problem of energy shortage in the future. The concept and potential use of integrated cleaner photo-technology with monolith photoreactor and low-cost photo-catalyst, here begun with CO_2 utilization, can be further expanded to other chemical production from greenhouse gases.

Acknowledgement

This work was supported by Ministry of Higher Education Malaysia for the financial support of this research under FRGS (Fundamental Research Grant Scheme, Vote 4F876) and UTM (University Technology Malaysia under Research University Grant, Vote 17H06).

Appendix A. Supplementary data

Supplementary data related to this article can be found at https://doi.org/10.1016/j.jclepro.2017.09.118.

References

Alaba, P.A., Abbas, A., Daud, W.M.W., 2017. Insight into catalytic reduction of CO_2: catalysis and reactor design. J. Clean. Prod. 140, 1298–1312.
Ali, K.A., Abdullah, A.Z., Mohamed, A.R., 2017. Visible light responsive TiO2 nanoparticles modified using Ce and La for photocatalytic reduction of CO2: effect of Ce dopant content. Appl. Catal. A Gen. 537, 111–120.
Chen, R., Cheng, X., Zhu, X., Liao, Q., An, L., Ye, D., He, X., Wang, Z., 2017a. High-performance optofluidic membrane microreactor with a mesoporous CdS/TiO_2/SBA-15@carbon paper composite membrane for the CO_2 photoreduction. Chem. Eng. J. 316, 911–918.
Chen, Z., Ma, Y., Geng, B., Wang, M., Sun, X., 2017b. Photocatalytic performance and magnetic separation of TiO_2-functionalized γ-Fe_2O_3, Fe, and Fe/Fe_2O_3 magnetic particles. J. Alloys Compd. 700, 113–121.
Harifi, T., Montazer, M., 2014. Fe3+:Ag/TiO2 nanocomposite: synthesis, characterization and photocatalytic activity under UV and visible light irradiation. Appl. Catal. A Gen. 473, 104–115.
He, Z.Q., Tang, J.T., Shen, J., Chen, J.M., Song, S., 2016. Enhancement of photocatalytic reduction of CO_2 to CH_4 over TiO_2 nanosheets by modifying with sulfuric acid. Appl. Surf. Sci. 364, 416–427.
Jiao, J., Wei, Y., Zhao, Y., Zhao, Z., Duan, A., Liu, J., Pang, Y., Li, J., Jiang, G., Wang, Y., 2017. AuPd/3DOM-TiO2 catalysts for photocatalytic reduction of CO2: high efficient separation of photogenerated charge carriers. Appl. Catal. B Environ. 209, 228–239.
Kiatphuengporn, S., Donphai, W., Jantaratana, P., Yigit, N., Föttinger, K., Rupprechter, G., Chareonpanich, M., 2017. Cleaner production of methanol from carbon dioxide over copper and iron supported MCM-41 catalysts using innovative integrated magnetic field-packed bed reactor. J. Clean. Prod. 142, 1222–1233.
Kočí, K., Matějová, L., Kozák, O., Čapek, L., Valeš, V., Reli, M., Praus, P., Šafářová, K., Kotarba, A., Obalová, L., 2014. ZnS/MMT nanocomposites: the effect of ZnS loading in MMT on the photocatalytic reduction of carbon dioxide. Appl. Catal. B Environ. 158–159, 410–417.
Kong, L., Wang, C., Wan, F., Zheng, H., Zhang, X., 2017. Synergistic effect of surface self-doping and Fe species-grafting for enhanced photocatalytic activity of TiO_2 under visible-light. Appl. Surf. Sci. 396, 26–35.
Li, Y., Cai, X., Guo, J., Zhou, S., Na, P., 2015. Fe/Ti co-pillared clay for enhanced arsenite removal and photo oxidation under UV irradiation. Appl. Surf. Sci. 324, 179–187.
Mulewa, W., Tahir, M., Amin, N.A.S., 2017. MMT-supported Ni/TiO_2 nanocomposite for low temperature ethanol steam reforming toward hydrogen production. Chem. Eng. J. 326, 956–969.
Ola, O., Maroto-Valer, M., Liu, D., Mackintosh, S., Lee, C.-W., Wu, J.C.S., 2012. Performance comparison of CO2 conversion in slurry and monolith photoreactors using Pd and Rh-TiO2 catalyst under ultraviolet irradiation. Appl. Catal. B Environ. 126, 172–179.
Paulino, P.N., Salim, V.M.M., Resende, N.S., 2016. Zn-Cu promoted TiO2 photocatalyst for CO2 reduction with H2O under UV light. Appl. Catal. B Environ. 185, 362–370.
Tahir, B., Tahir, M., Amin, N.S., 2015a. Performance analysis of monolith photoreactor for CO_2 reduction with H_2. Energy Convers. Manage 90, 272–281.
Tahir, M., 2017. Synergistic effect in MMT-dispersed Au/TiO2 monolithic nanocatalyst for plasmon-absorption and metallic interband transitions dynamic CO2 photo-reduction to CO. Appl. Catal. B Environ. 219, 329–343.
Tahir, M., Amin, N.S., 2013. Photocatalytic reduction of carbon dioxide with water vapors over montmorillonite modified TiO2 nanocomposites. Appl. Catal. B Environ. 142–143, 512–522.
Tahir, M., Amin, N.S., 2016. Performance analysis of nanostructured NiO–In_2O_3/TiO_2 catalyst for CO_2 photoreduction with H_2 in a monolith photoreactor. Chem. Eng. J. 285, 635–649.
Tahir, M., Tahir, B., 2016. Dynamic photocatalytic reduction of CO_2 to CO in a honeycomb monolith reactor loaded with Cu and N doped TiO_2 nanocatalysts. Appl. Surf. Sci. 377, 244–252.
Tahir, M., Tahir, B., Amin, N.S., 2015b. Photocatalytic CO_2 reduction by CH_4 over montmorillonite modified TiO_2 nanocomposites in a continuous monolith photoreactor. Mater. Res. Bull. 63, 13–23.
Tahir, M., Tahir, B., Saidina Amin, N.A., Alias, H., 2016. Selective photocatalytic reduction of CO_2 by H_2O/H_2 to CH_4 and CH_3OH over Cu-promoted In_2O_3/TiO_2 nanocatalyst. Appl. Surf. Sci. 389, 46–55.
Tong, Y., Chen, L., Ning, S., Tong, N., Zhang, Z., Lin, H., Li, F., Wang, X., 2017. Photocatalytic reduction of CO2 to CO over the Ti–Highly dispersed HZSM-5 zeolite containing Fe. Appl. Catal. B Environ. 203, 725–730.
Xiong, Z., Lei, Z., Ma, S., Chen, X., Gong, B., Zhao, Y., Zhang, J., Zheng, C., Wu, J.C.S., 2017a. Photocatalytic CO2 reduction over V and W codoped TiO2 catalyst in an internal-illuminated honeycomb photoreactor under simulated sunlight irradiation. Appl. Catal. B Environ. 219, 412–424.
Xiong, Z., Lei, Z., Xu, Z., Chen, X., Gong, B., Zhao, Y., Zhao, H., Zhang, J., Zheng, C., 2017b. Flame spray pyrolysis synthesized ZnO/CeO_2 nanocomposites for enhanced CO_2 photocatalytic reduction under UV–Vis light irradiation. J. CO2 Util. 18, 53–61.
Yang, M.-Q., Xu, Y.-J., 2016. Photocatalytic conversion of CO_2 over graphene-based composites: current status and future perspective. Nanoscale Horiz. 1, 185–200.
Yong, J.Y., Klemeš, J.J., Varbanov, P.S., Huisingh, D., 2016. Cleaner energy for cleaner production: modelling, simulation, optimisation and waste management. J. Clean. Prod. 111, 1–16.
Yu, W., Xu, D., Peng, T., 2015. Enhanced photocatalytic activity of g-C_3N_4 for selective CO_2 reduction to CH_3OH via facile coupling of ZnO: a direct Z-scheme mechanism. J. Mater. Chem. A 3, 19936–19947.
Yuan, K., Yang, L., Du, X., Yang, Y., 2014. Performance analysis of photocatalytic CO_2 reduction in optical fiber monolith reactor with multiple inverse lights. Energy Convers. Manage. 81, 98–105.
Zhu, Z., Qin, J., Jiang, M., Ding, Z., Hou, Y., 2017. Enhanced selective photocatalytic CO_2 reduction into CO over Ag/CdS nanocomposites under visible light. Appl. Surf. Sci. 391, 572–579.